Modelling the reservoir-to-tubing pressure drop imposed by multiple autonomous inflow control devices installed in a single completion joint in a horizontal well

Qinghua Lei [a,b*], Matthew D. Jackson [a], Ann H. Muggeridge [a], Pablo Salinas [a], Christopher C. Pain [a], Omar K. Matar [c], Kristine Årland [d]

[a] *Department of Earth Science and Engineering, Imperial College London, UK*

[b] *Department of Earth Sciences, ETH Zürich, Switzerland*

[c] *Department of Chemical Engineering, Imperial College London, UK*

[d] *Equinor ASA, Norway*

1. Introduction

Horizontal or highly deviated wells with long completions that are open to flow are used to increase the contact between the well and the hydrocarbon-bearing reservoir (Joshi, 1991). However, these wells can suffer from non-uniform inflow rates along the open completion, which results in early breakthrough of unwanted fluid phases such as gas or water. This is due to:

(1) the so-called 'heel-toe' effect (Birchenko et al., 2010; Dilib and Jackson, 2013), caused when a significant frictional pressure drop occurs along the production tubing, leading to a lower tubing pressure and, therefore, a larger reservoir pressure drawdown at the heel of the well as compared to the toe, and

(2) permeability variations along the well caused by reservoir heterogeneity (Dilib et al., 2012; Dilib and Jackson, 2013). The exact pattern of this permeability heterogeneity around any given well is generally uncertain.

* Correspondence: qinghua.lei@erdw.ethz.ch (Q. Lei)

Such non-uniform inflow and pre-mature breakthrough of unwanted fluids can have a negative impact on well productivity, well life and hydrocarbon recovery (Dilib et al., 2012).

Engineers may use inflow control devices to try to counteract the negative consequences of this non-uniform inflow. In this case, the outer annulus of the well is subdivided into a number of isolated zones using packers, and the inner annulus is then similarly subdivided into isolated completion joints, because early breakthrough of unwanted fluids at the well is likely to be restricted to just one or a few completion joints (Mathiesen et al., 2011; Ouyang, 2009). Inflow control devices are then installed in each isolated completion joint to passively or actively control inflow from the reservoir, by restricting flow from the annulus into the production tubing (Birchenko et al., 2011; Dilib and Jackson, 2013).

Passive inflow control devices (ICDs) impose a fixed additional pressure drop from the reservoir into the tubing to counteract the heel-toe effect however they suppress the flow of all fluid phases, including the oil (Dilib and Jackson, 2013; Ouyang, 2009). Furthermore, the sizing of these devices is usually based on the initial conditions along the production well, which may be significantly different from the time-varying behaviour during long-term operation (Dilib et al., 2012; Dilib and Jackson, 2013; Ouyang, 2009).

Alternatively autonomous inflow control devices (AICDs) provide active inflow control that can respond to the time-varying behaviour of the reservoir-well system. They are designed to introduce a pressure drop that varies depending on the volume fraction and flow rate of the different fluid phases entering the device. Typically, a larger pressure drop is applied to unwanted phases such as water or gas. AICDs are thus able to selectively choke unwanted fluid phases at the locations along the wellbore where they break through and their performance changes in response to time-varying reservoir behaviour. (Eltaher et al., 2014; Halvorsen et al., 2012; Mathiesen et al., 2011; Prebeau-Menezes et al., 2013).

The additional pressure drop imposed by a single AICD valve is measured typically in laboratory experiments for a range of fluid properties, total flow rates, and individual fluid phase flow rates or volume fractions. These data are then used to derive empirical relationships for the pressure drop using adjustable variables that are fitted to the measurements (Halvorsen et al., 2012; Mathiesen et al., 2011). These experimentally derived mathematical expressions are then implemented into a reservoir simulator to capture the effect of AICD valves on inflow to the well and evaluate the overall recovery efficiency and production performance (e.g. Eltaher et al., 2019). For example, Halvorsen et al. (2012) implemented the empirical equations into the reservoir simulation software Eclipse™ and predicted that a significant increase of oil production can be achieved by installing AICDs at the Troll field. Leitao Junior and Negrescu (2013) employed the similar approach to assess the oil production at the Peregrino field. Aakre et al. (2018) used the well completion simulation tool NETool, which assumes steady-state one-dimensional (1-D) flow and incorporates the experimentally based empirical equations, for analysing the performance of oil recovery at the Midale field. Eltaher et al. (2019) proposed a simplified formula fitting to experimental data and applied it for optimising the inflow control design.

These laboratory experiments are expensive, as they require specialist equipment and staff, occupy significant space in a laboratory and are time consuming to perform. Consequently some researchers have attempted to derive the additional pressure drop based on direct numerical simulation of fluid flow through a single AICD device (Zeng et al., 2015). These simulations can be computationally very expensive and still need to be properly validated by comparison with experiments.

In many cases, it may be necessary to install two or more AICDs in a single completion joint (Luo et al., 2015; Ostrowski et al., 2010; Youngs et al., 2009) in order to achieve desired inflow performance, however multiple AICDs can change the flow patterns (i.e. different from those for a single AICD) in the annulus. This means that the empirical relationships determined by fitting to experimental data for a single AICD, may no longer properly capture the total pressure drop from the annulus into the tubing. Direct use of these experimentally-derived equations for a single AICD to calculate the pressure drop imposed by multiple AICDs could cause significant inaccuracies in the predictions of reservoir simulation models. Thus, it is practically useful to develop an approach to extend the predictability of these formulations (e.g. by including a prefactor) for analysing production systems with multiple AICDs installed in each single completion joint.

This paper investigates the flow patterns resulting from two interacting AICDs and develops a modified pressure versus water cut relationship for these cases. We use state-of-the-art, high resolution numerical modelling techniques to capture the detailed physics and dynamics of multiphase flow in the inner annulus of a completion joint mounted with one or two AICD(s). Earlier work has shown that our numerical modelling techniques can capture the dynamics of multiphase flow in thin annuli, through comparison with experiments (Lei et al., 2018). The model is used to explore a range of relevant flow conditions with different flow rates and phase volume fractions and allows us to determine the pressure drop from the annulus to the tubing across one or two AICD(s). We focus here on oil-water flow, but the methods are equally applicable to oil-gas and gas-water flows; they are also equally applicable to study joints with three or more AICDs installed.

2. Wellbore configuration and autonomous inflow control devices

We study a typical wellbore configuration with inflow control (Fig. 1). The production well is divided into a number of isolated completion joints so that annular flow between neighbouring joints is eliminated. Each joint (12 m long) includes an outer, gravel-packed annulus, a mesh screen for sand control and a pipe section (Fig. 2). The pipe section has an inner annulus region (5 m long) through which fluids are transported into the tubing, and a closed region (7 m long) encapsulating the tubing but having no communication with the surrounding gravel pack. The inner annulus is enclosed by a sand screen, and part of it (4.5 m long) is partitioned into 48 parallel, narrow channels which restrict radial flow around the inner annulus. The rest of the inner annulus (0.5 m long) has no partitions and hosts the AICD(s). Table 1 summarises the geometric parameters of each component of the wellbore system. During production, oil and water flow from the surrounding reservoir rock into the outer annulus, across the sand screen, into the inner annulus and enter the tubing via the AICD(s) (see arrows in Fig. 2).

We focus on the two-phase flow of oil and water. The fluid properties are given in Table 2. We assume that the AICD valve imposes an additional pressure drop Δp_{AICD} on the oil-water mixture as it flows through the device, given by the empirical formula (Aakre et al., 2018; Eltaher et al., 2014; Halvorsen et al., 2012; Mathiesen et al., 2011):

$$\Delta p_{\mathrm{AICD}} = \left(\frac{\rho^2}{\rho_{\mathrm{cal}}}\right)\left(\frac{\mu_{\mathrm{cal}}}{\mu}\right)^n a_{\mathrm{AICD}} q_{\mathrm{AICD}}^m , \tag{1}$$

where a_{AICD} is the strength parameter of the AICD, q_{AICD} is the total flow rate into the AICD, m is the volume exponent, and n is the viscosity ratio exponent, ρ_{cal} and μ_{cal} are the calibration density and calibration dynamic viscosity, respectively, while ρ and μ are the density and dynamic viscosity of the oil-water mixture, respectively, given as (Aakre et al., 2018; Halvorsen et al., 2012; Mathiesen et al., 2011):

$$\rho = \alpha_{\mathrm{o}}\rho_{\mathrm{o}} + \alpha_{\mathrm{w}}\rho_{\mathrm{w}} , \tag{2}$$

$$\mu = \alpha_{\mathrm{o}}\mu_{\mathrm{o}} + \alpha_{\mathrm{w}}\mu_{\mathrm{w}} , \tag{3}$$

where α_{o} and α_{w} are the volume fractions of oil and water, respectively; ρ_{o} and ρ_{w} are the densities of oil and water, respectively. The parameters of a typical AICD valve obtained by fitting to laboratory data (modified based on (Aakre et al., 2018) and used in this study) are given in Table 3.

3. Numerical modelling methodology

3.1 Modelling of the inner annulus

To elucidate the impact of more than one AICD per completion joint on oil-water flow in the production system, we explicitly modelled the complex multiphase flow dynamics in a 2D model of the horizontally placed inner annulus with two AICD valves.

The 3-D problem was reduced to a two-dimensional (2-D) model (Fig. 3) associated with a distorted gravity field (Fig. 3c) (see (Lei et al., 2018) for the derivation details) by averaging across the annulus gap. Fig. 3a, shows the full, three dimensional (3-D), curvilinear coordinate system (x, y, z). The x coordinate was defined to be along the pipe length ($0 \leq x \leq L_i$), whilst y was around the perimeter ($-\pi D_i/2 \leq y \leq \pi D_i/2$ with y = 0 and $y = \pm \pi D_i/2$ corresponding to the top and bottom of the annulus, respectively, and D_i being the mean diameter of the pipe). The z coordinate thus measures the distance across the annulus, where the origin for the z coordinate was along the mid-plane of the inner annulus. The thickness of the annulus was h so the distance of this mid-plane from both the outer and inner walls was $h_i/2$. We assumed that the flow velocity in the z direction was negligible ($u_z = 0$). The annulus surfaces were assumed to be neutrally wetting for oil and water phases (i.e. not strongly wetted by either fluid with a contact angle of 90º), and laminar flow was assumed through the annulus meaning that the velocity profile was parabolic in the z direction (Gondret and Rabaud, 1997).

The derived gap-averaged governing equations are presented in the following subsection. The validity of this 2-D representation was determined by comparing the flow patterns it predicts with those seen in experiments (Lei et al. 2018). More details can also be found in the supplementary material.

3.2 Governing equations

The gap-averaged governing equations (Lei et al., 2018) for compressible two-phase, oil-water flow are given below. By conservation of volume, the sum of the volume fractions must sum to 1:

$$\alpha_{\mathrm{o}} + \alpha_{\mathrm{w}} = 1. \tag{4}$$

The equations for the conservation of mass for oil and water phases are:

$$\frac{\partial}{\partial t}(\alpha_{\mathrm{o}}\rho_{\mathrm{o}}) + \nabla \cdot (\alpha_{\mathrm{o}}\rho_{\mathrm{o}}\mathbf{u}) = 0, \tag{5}$$

and

$$\frac{\partial}{\partial t}(\alpha_{\mathrm{w}}\rho_{\mathrm{w}}) + \nabla \cdot (\alpha_{\mathrm{w}}\rho_{\mathrm{w}}\mathbf{u}) = 0, \tag{6}$$

respectively. The equation of motion is

$$\frac{\partial}{\partial t}(\rho\mathbf{u}) + \frac{6}{5}\nabla \cdot (\rho\mathbf{u} \otimes \mathbf{u}) = -\nabla p + \nabla \cdot \mu\left[\nabla\mathbf{u} + (\nabla\mathbf{u})^{\mathrm{T}}\right] - f\mathbf{u} + \rho\mathbf{g} + \sigma\kappa\delta\mathbf{n}. \tag{7}$$

Here, $\mathbf{u} = [u_{\mathrm{x}}, u_{\mathrm{y}}]$ is the gap-averaged velocity vector, $\nabla = [\partial/\partial x, \partial/\partial y]$ is the 2-D gradient, t is the time, the bulk density is $\rho = \alpha_{\mathrm{o}}\rho_{\mathrm{o}} + \alpha_{\mathrm{w}}\rho_{\mathrm{w}}$, p is the pressure, the bulk dynamic viscosity is $\mu = \alpha_{\mathrm{o}}\mu_{\mathrm{o}} + \alpha_{\mathrm{w}}\mu_{\mathrm{w}}$, the gravitational acceleration vector is $\mathbf{g} = [0, g\sin(2y/D_{\mathrm{i}})]$, f is the coefficient of frictional pressure loss (equal to $12\mu/h_{\mathrm{i}}^2$ for the flow in the non-partitioned inner annulus and $32\mu/d_{\mathrm{c}}^2$ for the flow in the narrow channels), σ is the surface tension, κ is the interface curvature, δ is the Dirac delta function, and $\mathbf{n}$ is the interface outward-pointing unit normal. Surface tension is treated as a continuous surface force (Brackbill et al., 1992). The densities of compressible oil and water are calculated respectively using:

$$\rho_{\mathrm{o}} = \frac{\rho_{\mathrm{o0}}}{1 - c_{\mathrm{o}}(p - p_0)}, \tag{8}$$

and

$$\rho_{\mathrm{w}} = \frac{\rho_{\mathrm{w0}}}{1 - c_{\mathrm{w}}(p - p_0)}, \tag{9}$$

where c_{o} and c_{w} are the compressibility coefficients of oil and water, respectively, and ρ_{o0} and ρ_{w0} are their densities at the reference tubing pressure p_0.

3.3 Initial and boundary conditions on flow into the inner annulus

Fig. 4 shows the 2D geometry used to simulate the fluid flow in the inner annulus with one or two AICD valves. The fluids enter the model via 48 narrow, parallel channels and are produced from one or two model AICDs placed within the annulus.

We assume that the flow through each channel is approximately 1D due to the high aspect ratio of the channels and approximate the flow entering these channels from the outer annulus as distributed inflow along the length of each channel. The velocity of the imposed distributed inflow varied linearly along each boundary from zero at the end furthest from the AICD to a maximum at the end of the channel nearest to the AICD (Figs. 4a and b). We further assume that the oil and water are completely segregated by gravity as they approach the sand-screen from the outer annulus so that there is single-phase flow within each channel i.e. each channel contains only water or only oil. As water is denser than oil, the default condition is that water enters through channels closest to the base, and oil enters through channels nearest the top. We investigated the sensitivity of the results to this by testing the opposite end-member scenario, in which oil entered at the base, and water entered at the top. This did not materially alter the results. The inflow rates from the reservoir are assumed to be steady because the timescales over which multiphase flow evolves in the annulus and the reservoir are very different. Steady flow for a given inflow and AICD configuration occurs over the timescale of seconds, compared to hours to years in the reservoir.

We explored two inflow rate cases of Q_{tot} = 20 and 30 m^3/day per completion joint, which correspond to approximately 125 bbl/day/joint and 187.5 bbl/day/joint, respectively, or approximately 10,000 – 15,000 bbl/day for a total well completion length of 1 km. The Reynolds numbers of the flow in the annulus for these two inflow rate cases were $\rho_{\mathrm{w0}}Q_{\mathrm{tot}}(2h_{\mathrm{i}})/\mu_{\mathrm{w}}/(\pi D_{\mathrm{i}}h_{\mathrm{i}})$ = 21.9 and 32.8, confirming that the flow is laminar (Beavers et al., 1970). We also examined a range of water cuts between 0 and 1 by adjusting the inlet boundary condition such that water flowed into more channels to yield a higher water cut, and fewer channels to yield a lower water cut, while oil flowed into the remaining channels.

We defined the initial volume fraction of fluids inside the annulus based on the corresponding water cut value. A free-slip condition was used for the two longitudinal sides of the (unrolled) domain.

We did not include an explicit model of the flow through each AICD valve in the simulation but instead represented their effect on the flow via an outlet pressure boundary in the shape of a square. The pressure around the border of each square varied depending upon the amount of water and oil flowing across that boundary and was calculated as the sum of the reference tubing pressure p_0 (constant) and the pressure drop imposed by the AICD, Δp_{AICD}, (Eq. 1). The first AICD was always located in the middle of the inner annulus domain (Fig. 4a) whilst the second AICD, if present, was located across the free slip boundary (see Fig. 4b). This meant it was decomposed into two parts, located on opposing lateral boundaries of the domain (Fig. 4b). An identical pressure for the two parts was enforced based on the overall flow across this AICD. The remaining boundaries of the domain were no-flow perpendicular to the boundary.

3.4 Numerical methods

The governing equations were solved using a mixed control-volume finite-element method, which has been validated against a series of benchmark cases of single rising bubbles, coalescence of two bubbles and droplet impacts (Xie et al., 2017, 2016, 2014). The computational domain was discretised using an unstructured grid of triangular $P_1DG\text{-}P_2$ elements (Cotter et al., 2009). A finite volume discretisation of the mass conservation equation and a linear discontinuous Galerkin discretisation of the momentum equation were used with an adaptive implicit/explicit time stepping scheme (Xie et al., 2016). Within each time step, the equations were iterated using a pressure projection method until all equations are simultaneously balanced (Pavlidis et al., 2014; Xie et al., 2014). The interface dynamics were captured through a compressive advection-based volume-of-fluid approach, which uses a novel and mathematically rigorous nonlinear Petrov-Galerkin method for maintaining sharp interfaces (Pavlidis et al., 2016). Surface tension was modelled using a diffused-interface formulation based on the volume fraction field (Xie et al., 2016). The numerical algorithm is summarised in Fig. 6.

The simulation used a fixed mesh with different discretisation settings for different subdomains (Fig. 5b). In the narrow channels, a structured mesh was used with element edge lengths in the tangential and longitudinal directions of 0.002 m and 0.1 m, respectively (a much larger element size was used for the longitudinal direction to reduce computational costs without violating the model accuracy). Our numerical solver is sufficiently robust that it can converge to a solution when such high aspect ratio elements are used (Xie et al., 2014). For the inner annulus hosting the AICD(s), an average element size of 0.002 m was used to build an unstructured mesh and a local refinement with average element sizes of 0.001 m was applied in the vicinity of the AICD(s). These values were chosen following a mesh sensitivity analysis (see the supplementary material for the details). The total number of elements was almost 60,000. An adaptive time stepping scheme was used that ensured all time-steps conformed to the Courant–Friedrichs–Lewy (CFL) condition with the CFL number being set to 1, i.e. time step $\Delta t \leq h/u$, where h is the local element size and u is the local fluid velocity. The run time for each simulation was about 600 hours on a desktop computer equipped with an Intel(R) Xeon(R) CPU E5-2697@2.30 GHz.

3.5 Model validation and verification

The flow dynamics in a cylindrical annulus for both oil-water and gas-water flow predicted by the numerical model have been previously validated by comparison against experimental results (Lei et al. 2018). A summary of the experimental setup and model validation results is also provided in the supplementary material.

In addition, we verified that the numerical model gave the same average pressure drops across the AICD as predicted by Eq. (1) for single-phase flow (water or oil) and two-phase oil-water flow (with a fixed water cut of 0.5) through a single AICD, for a range of flow rates. We measured the pressure drop averaged around the boundary of the AICD and the tubing, and then compared this with that predicted using Eq. (1). The very close match (Fig. 7) confirmed that the chosen outlet boundary conditions mimicked the flow rate and pressure drop behaviour as observed in a real AICD. There was a much higher pressure drop when water was flowing compared to oil, because the AICD was designed to choke-back the flow of water.

4. Simulation results

4.1 Single AICD

We first studied the fluid patterns obtained in a system with a single AICD together with the pressure drops across the AICD and the total flow rate and the oil and water flow rates through it, for a flow rate of Q_{tot} = 20 m^3/day and a range of water cuts (Fig. 8). Water entered the annulus from the base while oil entered from the top.

Fig. 8 shows the pressure drop measured across the AICD and the flow rates through it as a function of time. Steady-state flow was reached within 1.5 seconds in all cases (a very short timescale compared to the evolution of flow in the reservoir, which evolves over hours to years). Note that the total outflow rate across the AICD exhibited slight fluctuations because of the fluid compressibility and the choking-induced pressure variation.

Fig. 9 shows distribution of oil and water over time on the channels and the annulus at different times and water cuts. For low water cuts (e.g. 0.1), water that entered the annulus via the lower channels coned upwards to reach the AICD located at the top of the annulus (Fig. 9a). For intermediate water cuts (e.g. 0.5), the water cone became much wider, and approximately equal volumes of water and oil exited the annulus via the AICD (Fig. 9b). At high water cuts (e.g. 0.9), the water phase dominated the flow into the AICD (Fig.9c).

Fig. 10 gives the pressure drops across the AICD and flowrates through it for an injection rate of 30 m^3/day. There is a larger pressure drop across the AICD compared to that seen for Q_{tot} = 20 m^3/day (as expected) and again steady state is reached very quickly (~1 s). The flow patterns obtained for Q_{tot} = 30 m^3/day and the different water cuts were very similar to those for Q_{tot} = 20 m^3/day and are not shown here to avoid redundancy.

Fig. 11 compares the AICD pressure drops as a function of water cut obtained from simulation with those predicted by Eq. (1) when the AICD was located at the top or bottom of the annulus for the case when water entered the annulus from the bottom as well as the case when water entered from the top. Fig 11a shows the results for 20 m^3/day when water entered the annulus from the top and bottom. Fig. 11b show the results for the 30m^3/day flow rate case. All pressure drops were obtained after a simulation time of 1.5 s, when it was assumed that steady state had been achieved. The AICD pressure drop increased as the water cut increased, demonstrating its selective choking effect as expected. More importantly, there is good agreement between the numerical predictions and those obtained from the AICD formula (Eq. 1), irrespective of the position of the AICD and whether water entered the annulus from the base or top. The results confirm that the exact details of how water enters the inner annulus and the position of a single AICD have negligible effect on flow through, and the pressure drop across the AICD.

4.2 Two AICDs

We next investigated the oil-water flow in an annulus with two AICDs, one located at the top of the annulus and one at the base.

Fig. 12 shows the simulation results of flow rate and pressure drop for the case of Q_{tot} = 20 m^3/day, Again, steady state was reached after around 0.2-1.5 seconds. As expected, the pressure drops imposed by each AICD increases with water cut. At the lowest water cut the pressure drop across the lower AICD is slightly higher than that of the upper AICD suggesting there is more water flowing into the lower AICD while the total outflow rate from the upper AICD was higher than that of the lower AICD. This difference in pressure drops across the AICDs increases for the intermediate water cut case (0.5) and then decreases again for the highest water cut case (0.9).

Fig. 13 shows the oil and water distribution seen around the top and bottom AICDs as a function of time for different water cuts. When the water cut was low (e.g. 0.1), the water phase, which occupied the lower part of the annulus, left the annulus only via the lower AICD (Fig. 13a). The upper AICD is surrounded by oil and the lower AICD is also mostly surrounded by oil. This is consistent with the lower pressure drops measured across both AICDs and the slightly higher pressure drop see across the lower AICD (Fig 12a). For intermediate water cuts (0.5), the lower AICD is surrounded by water. The water also cones up to partially outflow via the upper AICD (Fig. 13b). Again this is consistent with the increased pressure drop seen across both AICDs for this case, together with the larger difference in pressure drop seen across the lower AICD (Fig. 12b). For the highest water cut (0.9), the water phase completely surrounds the lower AICD and is also the dominant phase around the upper AICD (Fig.13c). Again, this is consistent with the pressure drops measured across each AICD (Fig. 12c)

Fig. 14 gives the simulation results for flow rate and pressure drop for the case of Q_{tot} = 30 m^3/day. As expected the pressure drops across the AICDs are higher than those obtained when Q_{tot} = 20 m^3/day. The flow pattern evolution for Q_{tot} = 30 m^3/day was very similar to that for Q_{tot} = 20 m^3/day and is not shown to avoid redundancy.

We analysed the variation of the absolute pressure in the annulus by plotting a polar diagram for the cross-section containing the two AICDs (Fig. 15). The pressure around the annulus is approximately uniform apart from close to the AICDs however, the magnitude of the pressure increases with water cut due to pressure around the boundary of both the AICDs increasing with water cut. There is a greater drawdown of pressure around the upper AICD for both the 0.5 and 0.9 water cut cases, because there is a higher flow rate of oil into this AICD (e.g. the top AICD in Fig. 12) so the pressure around the boundary of this AICD is lower. This indicates a self-organisation of the flow partitioning between the two AICDs resulting in the oil-water flow pattern in the annulus tending towards a steady state.

Fig. 16 compares the simulated pressure drops across each AICD (calculated after 1.5 s when steady-state flow was achieved) with the predictions of Eq. 1 as a function of water cut for two different total flow rates. The results obtained when water enters the inner annulus from the top rather than the bottom are also shown. Unlike the single AICD case (Fig. 11) there is a marked difference between the results of the numerical simulation and the AICD equation, especially when the water cut is larger than 0.2. Not only are the pressure drops across both AICDs higher, there is a different pressure drop across each AICD. This is because there are different flows and water cuts into each AICD and the flow patterns of oil and water for the two AICD case (Fig. 13) are different from those seen in the single AICD case (Fig. 11). The simple mathematical calculation using Eq. (1) assumes that the flows into and around the two AICDs are identical and the flow pattern within the inner annulus is not altered by the presence of 2 AICDs. This difference is particularly noticeable when water cut is high. The results are very similar whether water enters the inner annulus from the top or bottom channels.

We calculated the average pressure drop between the annulus and the tubing and then computed the ratio η of this pressure drop derived from numerical simulation to the solution of the AICD formula for two different flow rates (Fig. 17). It can be seen that η is close to 1 when the water cut is smaller than 0.2, but abruptly increases to a maximum value of approximately 2.4 when the water cut is increased to around 0.3-0.4, beyond which η gradually decreases to 1 as the water cut approaches unity. The peak value of η tends to shift slightly to the left in Fig. 17 as the total flow rate increases, but the general variation of η seems to be reasonably independent of the total flow rate, at least for the two cases examined here. Importantly, the location of the AICD, and whether the water enters the annulus from the top or bottom, have a relatively small impact on the η value, as indicated by the shaded areas in Fig. 17. We suggest that the coefficient η may be used as a "correction factor" to the AICD formula to improve its predictability and assess the uncertainty when dealing with a completion joint with two AICDs.

5. Discussion

The correction factor, shown in Fig. 17, was derived assuming fully segregated inflow of water and oil into the completion joint. In reality, there may also be unsegregated flow occurring. Further detailed simulation work is needed to investigate the impact of these different inflow conditions, but capturing the dynamics of the oil-water interfaces in these complex flows would be very computationally expensive. We speculate that the behaviour of the completion system with unsegregated inflow will be bounded by the results of our numerical simulation assuming fully segregated inflow and the direct calculation by the AICD formula assuming fully mixed inflow. We suggest that the possible impact of these non-segregated flows on reservoir performance could be evaluated approximately by performing a sensitivity analysis using our simulation approach to derive the upper bound and the original AICD equation to calculate the lower bound.

It should be noted that the characteristic correction factor curve reported here will probably be affected by the intrinsic properties of the fluids and completion system, such as fluid viscosity, fluid density, the AICD design, number of AICDs and possibly the geometry of the inner annulus. Further simulation studies are needed to evaluate the impact of these factors on the shape and magnitude of the correction factor curve.

In the absence of these quantitative studies, our results indicate that the installation of 2 AICDs in a completion joint will significantly increase the pressure drop between the inner annulus and tubing at intermediate water cuts (between 0.3 and 0.6). This increase does not seem to depend on total flow rate into the joint. The possible impact of this pressure drop could be estimated by comparing simulation results using the single AICD formula with one in which the pressure drop is doubled for these intermediate water cuts.

6. Conclusions

In this paper, we have investigated, using detailed simulation of the flow in the annulus, how the oil-water flow pattern and associated pressure drop change when there are two AICDs in a completion joint rather than one. Our model has provided new insights into the flow interactions between the two AICDs. There is a different flow pattern around each AICD when there is two-phase flow in the annulus mounted with more than one AICDs. The interaction between the AICDs results in self-organised behaviour. It also results in a different average different pressure drop between the annulus and the tubing at intermediate water cuts when there are two AICDs in the annulus rather than one. This average pressure drop is higher than would be predicted, assuming the flow with two AICDs is identical to when there is a single AICD. We have quantified this discrepancy as a water cut-dependent correction to the AICD equation (derived in the literature for the case of single AICD) extending its predictability for the case of two AICDs. This correction could be used in reservoir simulation models to better capture the pressure drop across a single completion containing two AICDs.

Our modelling method also provides a generalised framework for exploring further scenarios, e.g. with even more AICDs mounted in a completion joint or different AICD types. Our investigations have shown that the detailed flow dynamics within the annulus can affect the well performance. Further research is needed to better understand these impacts.

Acknowledgements

We would like to acknowledge Statoil ASA (recently renamed as Equinor ASA) for funding Q.L., M.D.J., C.C.P., O.K.M. and A.H.M., and for granting permission to publish this work. O.K.M. and C.C.P. acknowledge the funding provided by the Engineering and Physical Sciences Research Council (EPSRC) through the Programme Grant MEMPHIS (grant EP/K003976/1). P.S. thanks ExxonMobil and the EPSRC (grant EP/R005761/1) for funding.

No data were generated in the course of this work. For further information, please contact the corresponding author Q.L. (email: qinghua.lei@erdw.ethz.ch), the AMCG Group (http://www.imperial.ac.uk/earth-science/research/research-groups/amcg/), the NORMS group (http://www.imperial.ac.uk/earth-science/research/research-groups/norms) or the Matar Fluids Group (http://www.imperial.ac.uk/matar-fluids-group).

References

Aakre, H., Mathiesen, V., Moldestad, B., 2018. Performance of CO2 flooding in a heterogeneous oil reservoir using autonomous inflow control. J. Pet. Sci. Eng. 167, 654–663. https://doi.org/10.1016/j.petrol.2018.04.008

Beavers, G.S., Sparrow, E.M., Magnuson, R.A., 1970. Experiments on the breakdown of laminar flow in a parallel-plate channel. Int. J. Heat Mass Transf. 13, 809–815. https://doi.org/10.1016/0017-9310(70)90127-4

Birchenko, V.M., Bejan, A.I., Usnich, A. V., Davies, D.R., 2011. Application of inflow control devices to heterogeneous reservoirs. J. Pet. Sci. Eng. 78, 534–541. https://doi.org/10.1016/j.petrol.2011.06.022

Birchenko, V.M., Muradov, K.M., Davies, D.R., 2010. Reduction of the horizontal well's heel–toe effect with inflow control devices. J. Pet. Sci. Eng. 75, 244–250. https://doi.org/10.1016/j.petrol.2010.11.013

Brackbill, J.., Kothe, D.., Zemach, C., 1992. A continuum method for modeling surface tension. J. Comput. Phys. 100, 335–354. https://doi.org/10.1016/0021-9991(92)90240-Y

Cotter, C.J., Ham, D.A., Pain, C.C., Reich, S., 2009. LBB stability of a mixed Galerkin finite element pair for fluid flow simulations. J. Comput. Phys. 228, 336–348. https://doi.org/10.1016/j.jcp.2008.09.014

Dilib, F.A., Jackson, M.D., 2013. Closed-loop feedback control for production optimization of intelligent wells under uncertainty. SPE Prod. Oper. 28, 345–357. https://doi.org/10.2118/150096-PA

Dilib, F.A., Jackson, M.D., Zadeh, A.M., Aasheim, R., Årland, K., Gyllensten, A.J., Erlandsen, S.M.,

2012. Closed-loop feedback control in intelligent wells: application to a heterogeneous, thin oil-rim reservoir in the North Sea. SPE Annu. Tech. Conf. Exhib. https://doi.org/10.2118/159550-ms

Eltaher, E., Muradov, K., Davies, D., Grassick, P., 2019. Autonomous flow control device modelling and completion optimisation. J. Pet. Sci. Eng. 177, 995–1009. https://doi.org/10.1016/j.petrol.2018.07.042

Eltaher, E.K., Muradov, K., Davies, D.R., Grebenkin, I.M., 2014. Autonomous inflow control valves - their modelling and "added value," in: SPE Annual Technical Conference and Exhibition. Society of Petroleum Engineers, pp. 27–29. https://doi.org/10.2118/170780-MS

Gondret, P., Rabaud, M., 1997. Shear instability of two-fluid parallel flow in a Hele–Shaw cell. Phys. Fluids 9, 3267–3274. https://doi.org/10.1063/1.869441

Halvorsen, M., Elseth, G., Nævdal, O.M., 2012. Increased oil production at Troll by autonomous inflow control with RCP valves. SPE Annu. Tech. Conf. Exhib. https://doi.org/10.2118/159634-ms

Joshi, S.D., 1991. Horizontal well technology. PennWell Corporation, Oklahoma.

Lei, Q., Xie, Z., Pavlidis, D., Salinas, P., Veltin, J., Matar, O.K., Pain, C.C., Muggeridge, A.H., Gyllensten, A.J., Jackson, M.D., 2018. The shape and motion of gas bubbles in a liquid flowing through a thin annulus. J. Fluid Mech. 855, 1017–1039. https://doi.org/10.1017/jfm.2018.696

Leitao Junior, I.L.F., Negrescu, M., 2013. ICD/AICD for heavy oil - technology qualification at the Peregrino field, in: Offshore Technology Conference. pp. 29–31. https://doi.org/10.4043/24503-MS

Luo, W., Li, H.T., Wang, Y.Q., Wang, J.C., 2015. A new semi-analytical model for predicting the performance of horizontal wells completed by inflow control devices in bottom-water reservoirs. J. Nat. Gas Sci. Eng. 27, 1328–1339. https://doi.org/10.1016/j.jngse.2015.03.001

Mathiesen, V., Werswick, B., Aakre, H., Elseth, G., 2011. Autonomous valve, a game changer of inflow control in horizontal wells., in: Offshore Europe. Society of Petroleum Engineers, p. 145737. https://doi.org/10.2118/145737-MS

~~Ostrowski, L.P., Galimzyanov, A.R., Uelker, B., 2010. Advances in modeling of passive inflow control devices help optimizing horizontal well completions, in: SPE Russian Oil and Gas Conference and Exhibition. Society of Petroleum Engineers, Moscow, Russia, p. 135998. https://doi.org/10.2118/135998-RU~~

Ouyang, L.-B., 2009. Practical consideration of an inflow-control device application for reducing water production, in: SPE Annual Technical Conference and Exhibition. Society of Petroleum Engineers, p. 124154. https://doi.org/10.2118/124154-MS

Pavlidis, D., Gomes, J.L.M.A., Xie, Z., Percival, J.R., Pain, C.C., Matar, O.K., 2016. Compressive advection and multi-component methods for interface-capturing. Int. J. Numer. Methods Fluids 80, 256–282. https://doi.org/10.1002/fld.4078

Pavlidis, D., Xie, Z., Percival, J.R., Gomes, J.L.M.A., Pain, C.C., Matar, O.K., 2014. Two- and three-phase horizontal slug flow simulations using an interface-capturing compositional approach. Int. J. Multiph. Flow 67, 85–91. https://doi.org/10.1016/j.ijmultiphaseflow.2014.07.007

Prebeau-Menezes, L., Mjolhus, S.J. de C., Liland, G., 2013. World’s first TAML Level 5 multi-lateral well with individual remote inflow control of three branches on Troll oil field, in: Offshore Technology Conference. Offshore Technology Conference, Rio de Janeiro, Brazil, p. 24427. https://doi.org/10.4043/24427-MS

Xie, Z., Hewitt, G.F., Pavlidis, D., Salinas, P., Pain, C.C., Matar, O.K., 2017. Numerical study of three-dimensional droplet impact on a flowing liquid film in annular two-phase flow. Chem. Eng. Sci.

166, 303–312. https://doi.org/10.1016/j.ces.2017.04.015

Xie, Z., Pavlidis, D., Percival, J.R., Gomes, J.L.M.A., Pain, C.C., Matar, O.K., 2014. Adaptive unstructured mesh modelling of multiphase flows. Int. J. Multiph. Flow 67, 104–110. https://doi.org/10.1016/j.ijmultiphaseflow.2014.08.002

Xie, Z., Pavlidis, D., Salinas, P., Percival, J.R., Pain, C.C., Matar, O.K., 2016. A balanced-force control volume finite element method for interfacial flows with surface tension using adaptive anisotropic unstructured meshes. Comput. Fluids 138, 38–50. https://doi.org/10.1016/j.compfluid.2016.08.005

Youngs, B., Neylon, K.J., Holmes, J.A., 2009. Recent Advances In Modeling Well Inflow Control Devices In Reservoir Simulation, in: International Petroleum Technology Conference. International Petroleum Technology Conference, pp. 1–6. https://doi.org/10.2523/13925-MS

Zeng, Q., Wang, Z., Wang, X., Wei, J., Zhang, Q., Yang, G., 2015. A novel autonomous inflow control device design and its performance prediction. J. Pet. Sci. Eng. 126, 35–47. https://doi.org/10.1016/j.petrol.2014.12.003

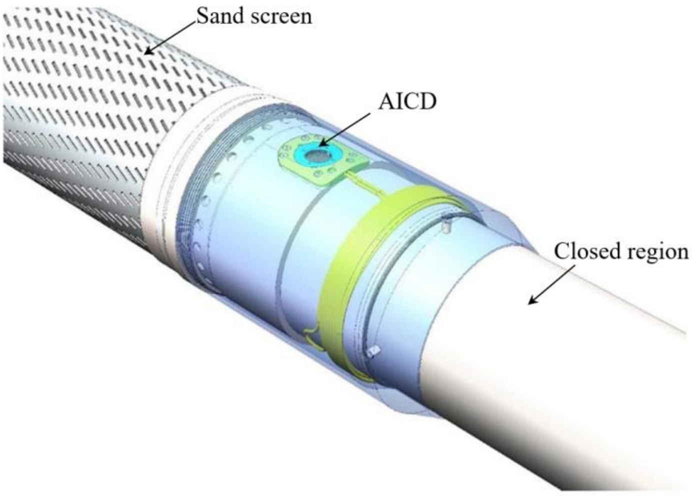

Fig. 1. A typical wellbore configuration, in which the AICD is mounted on the base pipe associated with a sand screen mesh (after Aakre et al., 2018).

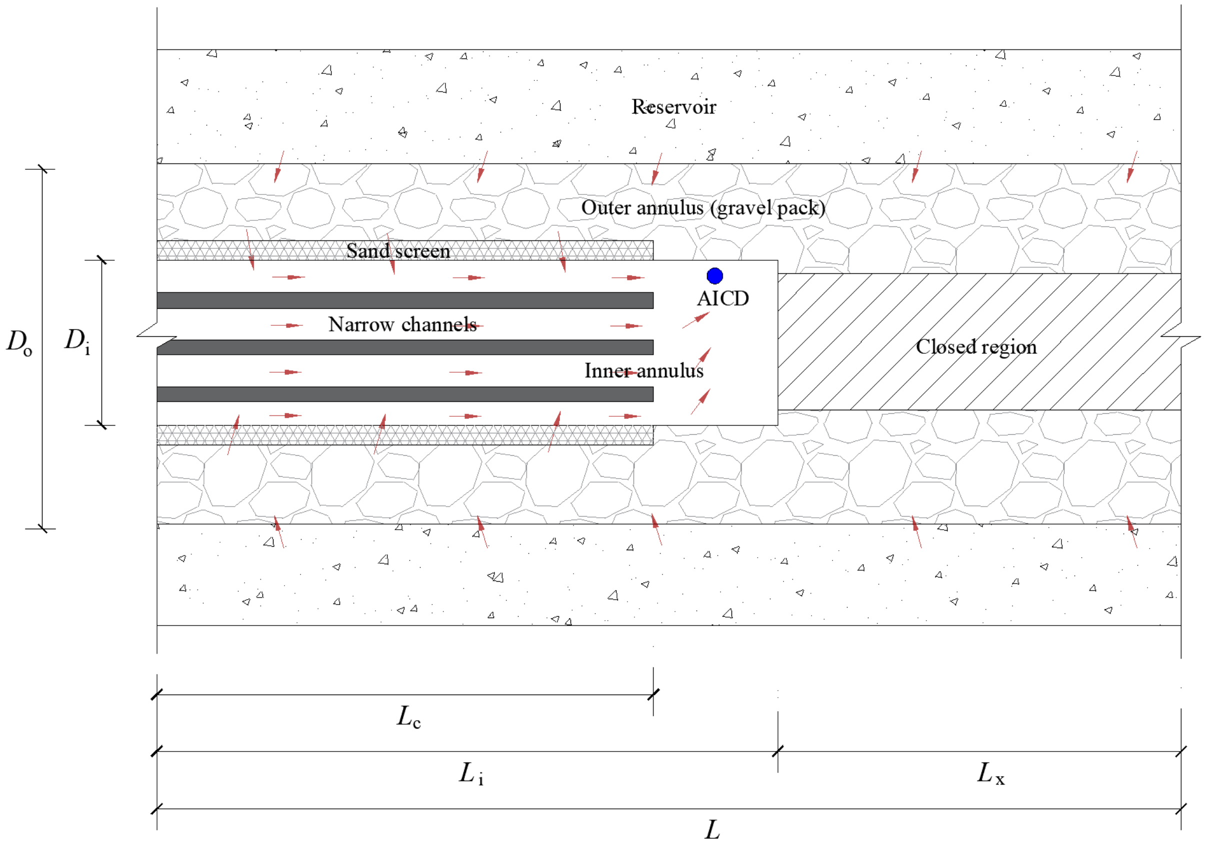

Fig. 2. Schematic showing the configuration of a completion joint for oil production in a hydrocarbon reservoir. The arrows indicate the direction of flow from the reservoir into the wellbore system, successively passing through the outer annulus (gravel pack), sand screen, inner annulus and AICD.

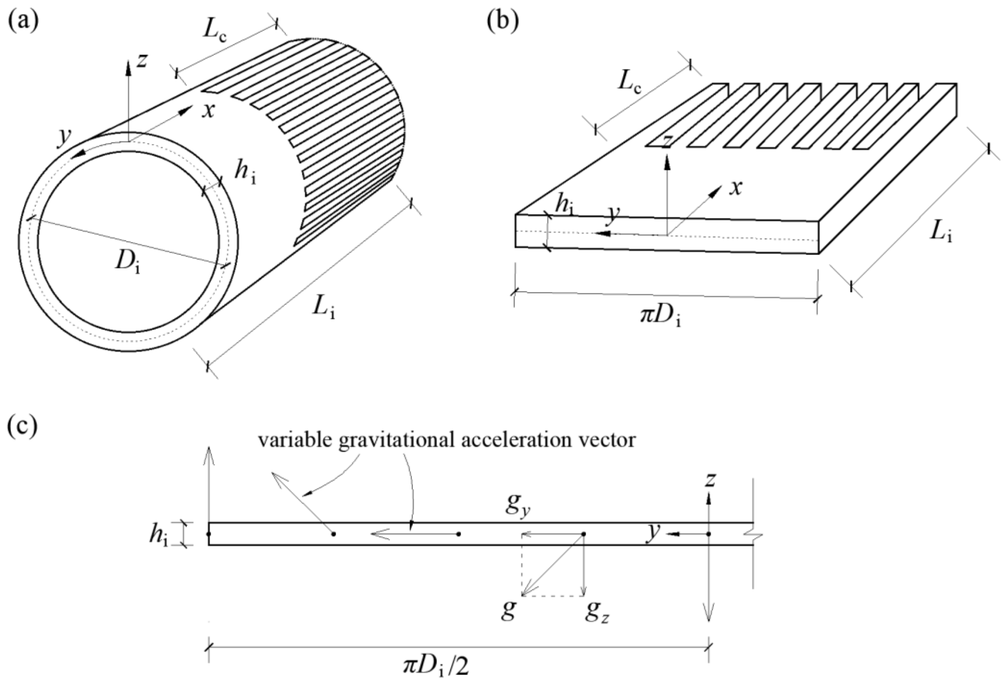

Fig. 3. Schematic of (a) the inner annulus and (b) the equivalent Hele-Shaw cell. (c) An illustration showing how the direction of gravitational acceleration changes along the equivalent Hele-Shaw cell to ensure the flow replicates that seen in the actual annulus.

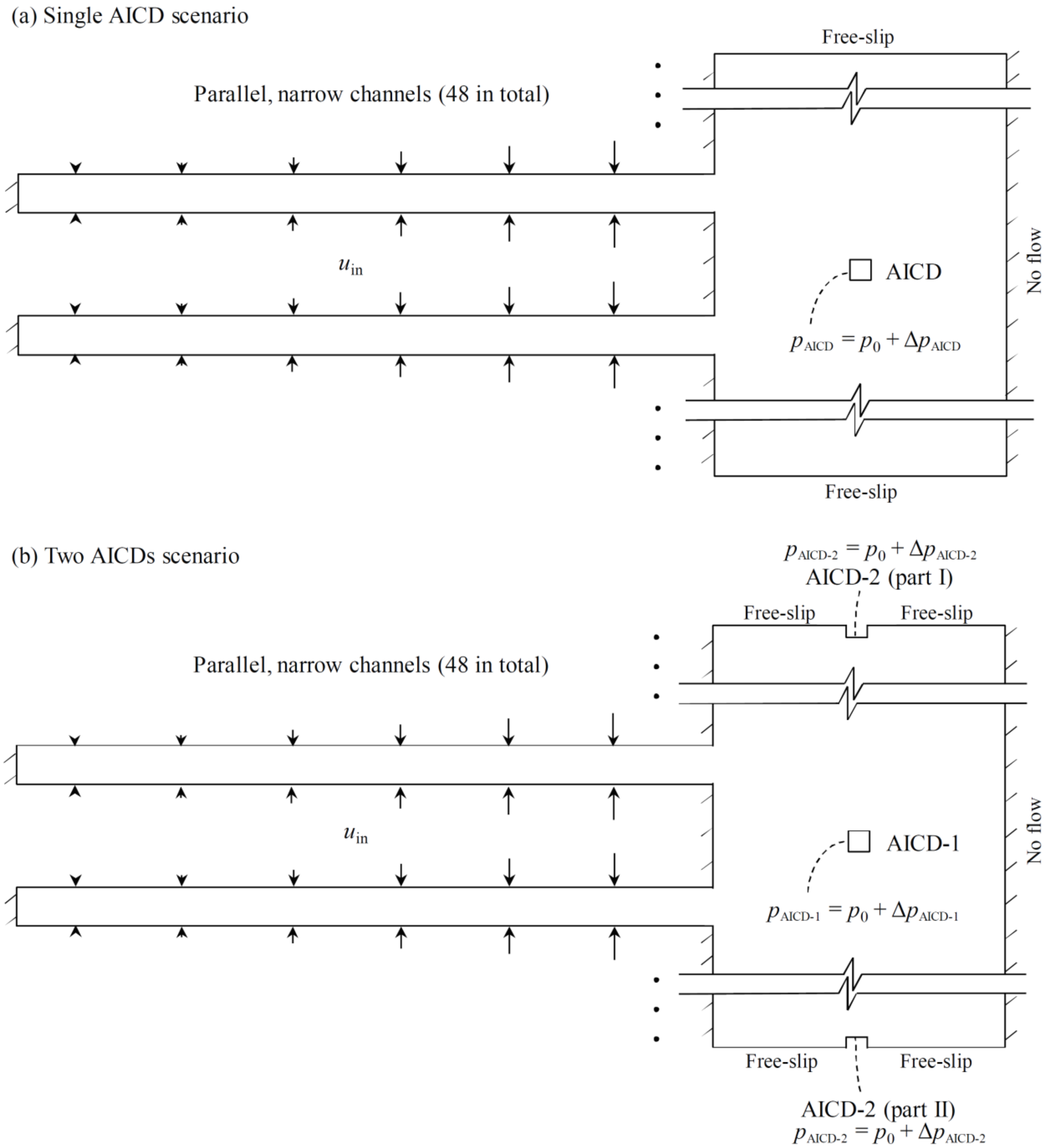

Fig. 4. Model representation and set-up for the inner annulus mounted with (a) a single AICD or (b) two AICDs.

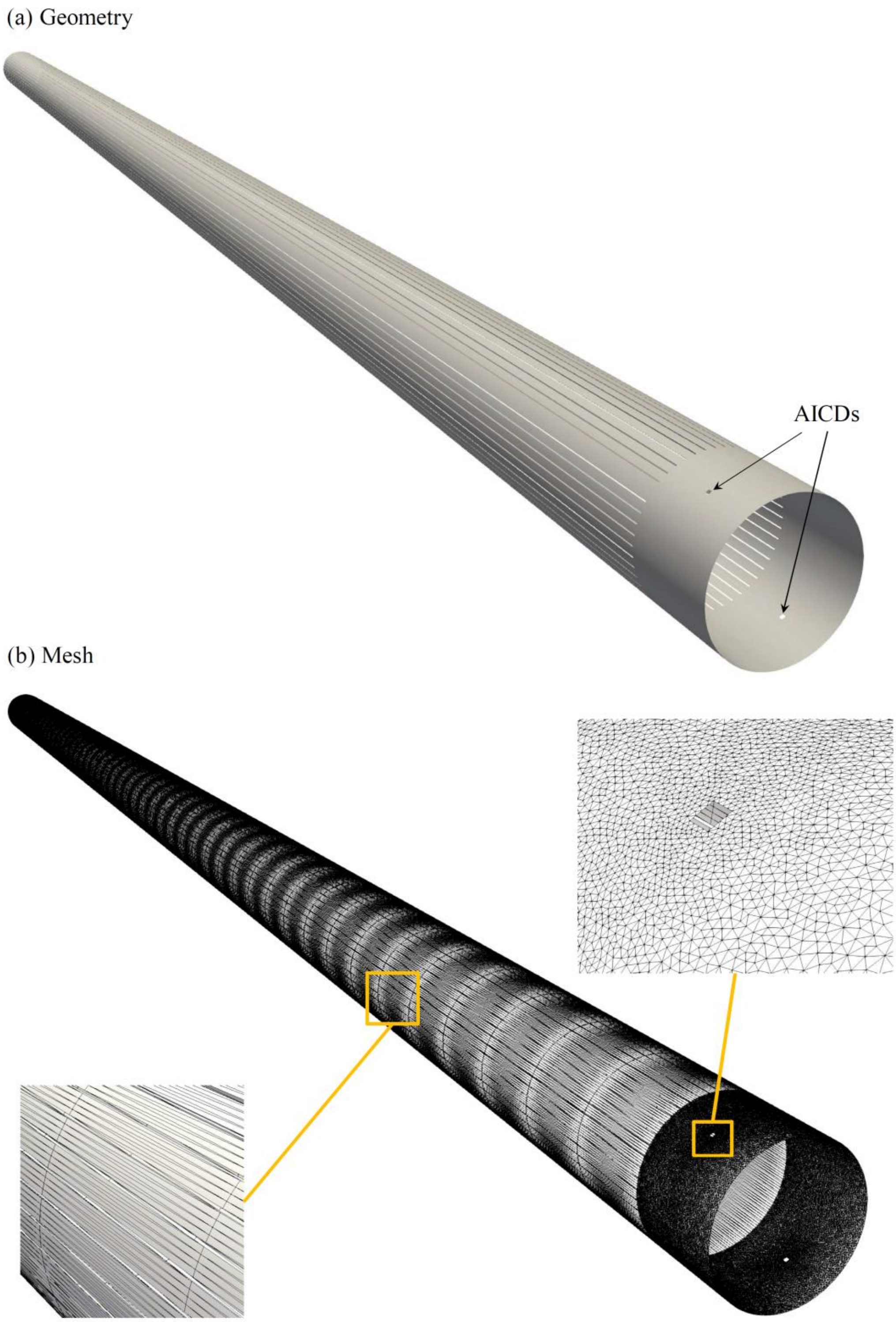

Fig. 5. (a) Geometry and (b) mesh of the 2-D numerical model projected onto the 3-D Cartesian coordinate system for visualisation.

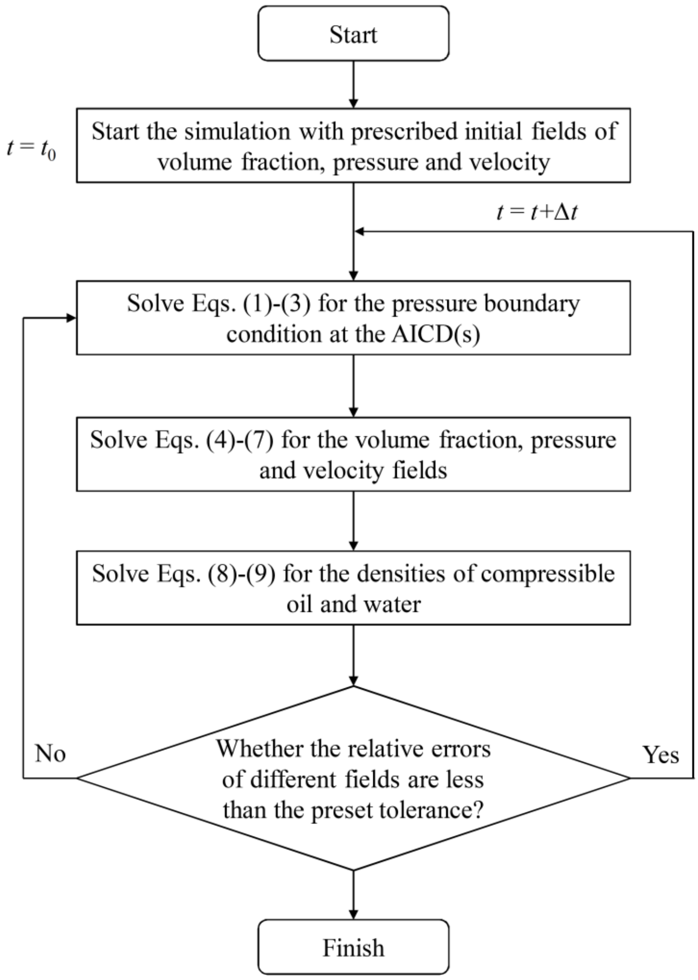

Fig. 6. Flowchart for the numerical calculation.

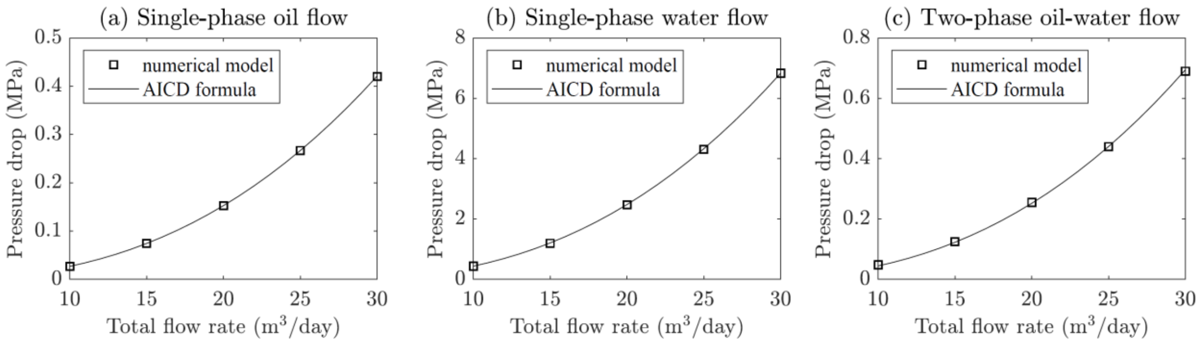

Fig. 7. Pressure drop imposed by the AICD for single-phase (a) oil or (b) water flow and (c) two-phase oil-water flow (with a water cut of 0.5) of different total flow rates.

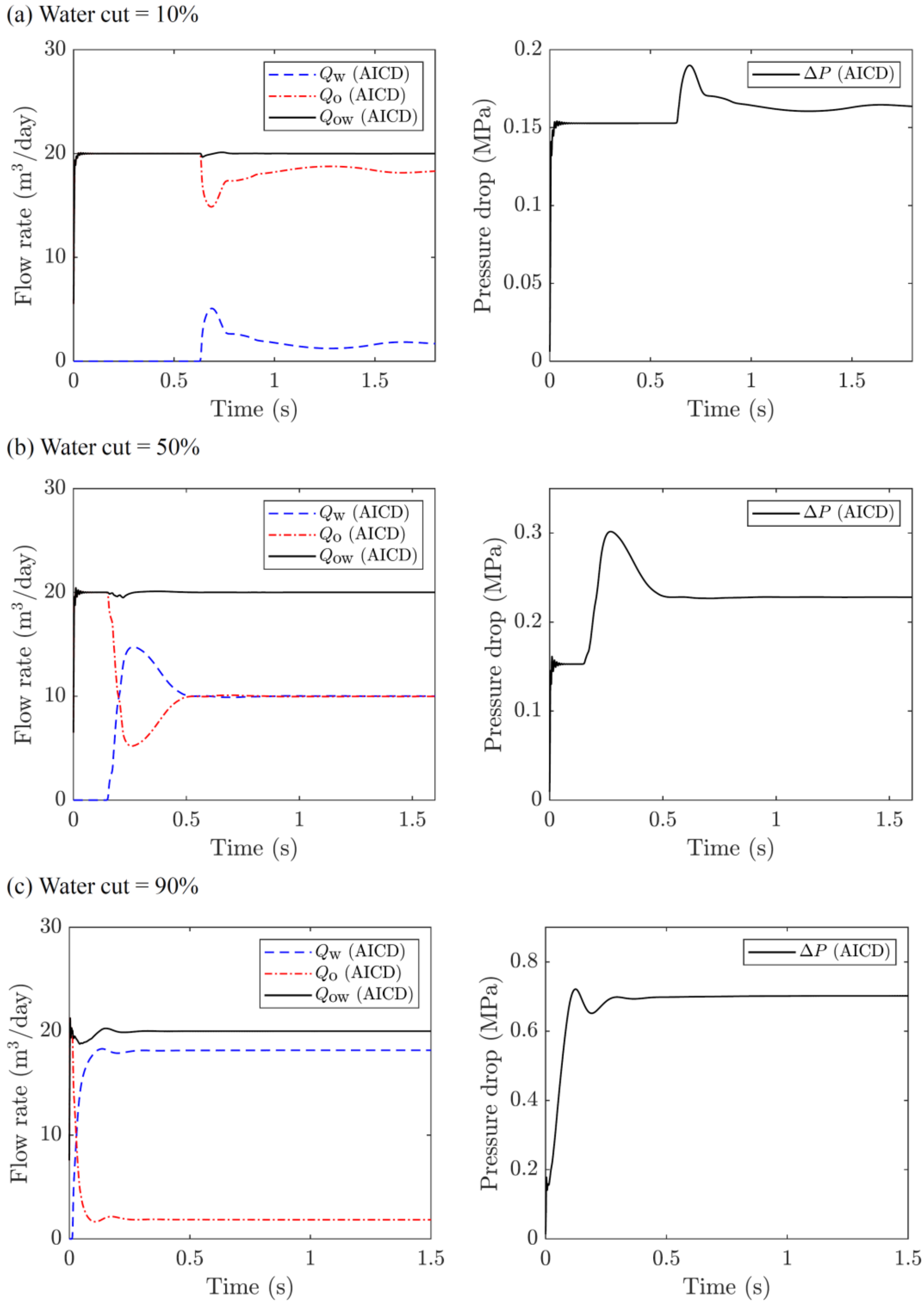

Fig. 8. Variation of flow rate (left) and pressure drop (right) at the AICD for different water cut cases with the total flow rate Q_{tot} = 20 m^3/day.

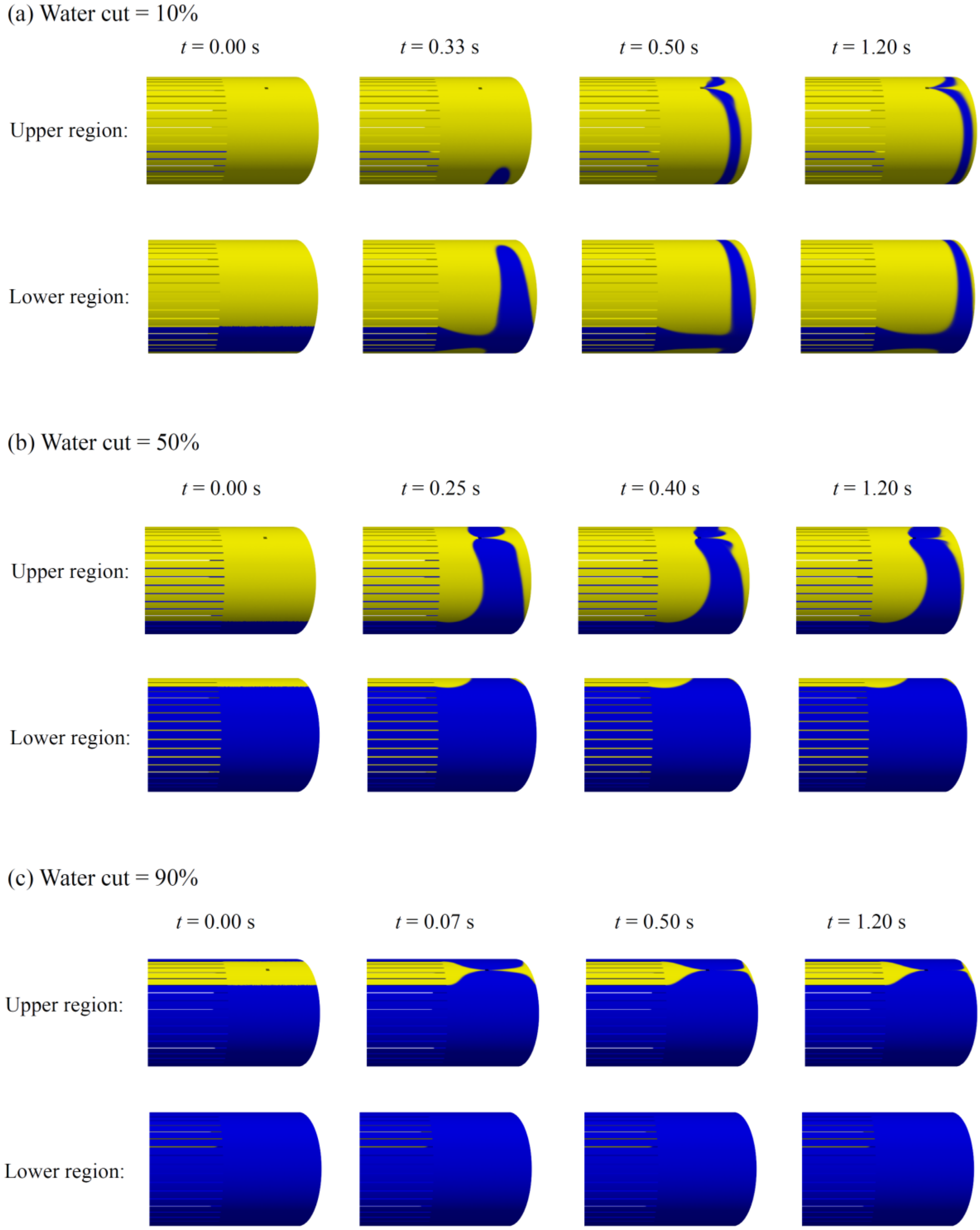

Fig. 9. Variation of flow pattern at the AICD for different water cut cases with the total flow rate Q_{tot} = 20 m^3/day.

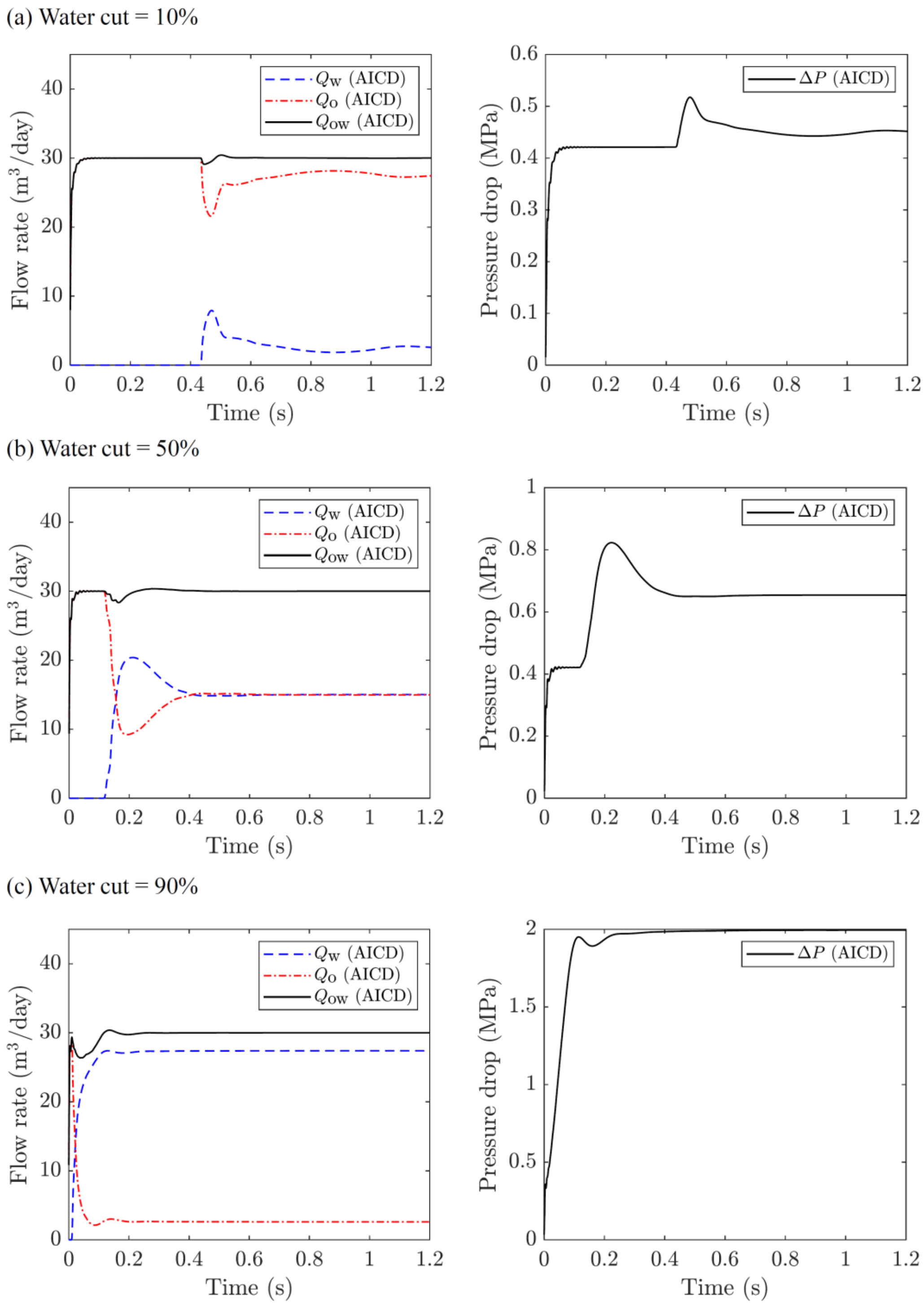

Fig. 10. Variation of flow rate (left) and pressure drop (right) at the AICD for different water cut cases with the total flow rate Q_{tot} = 30 m^3/day.

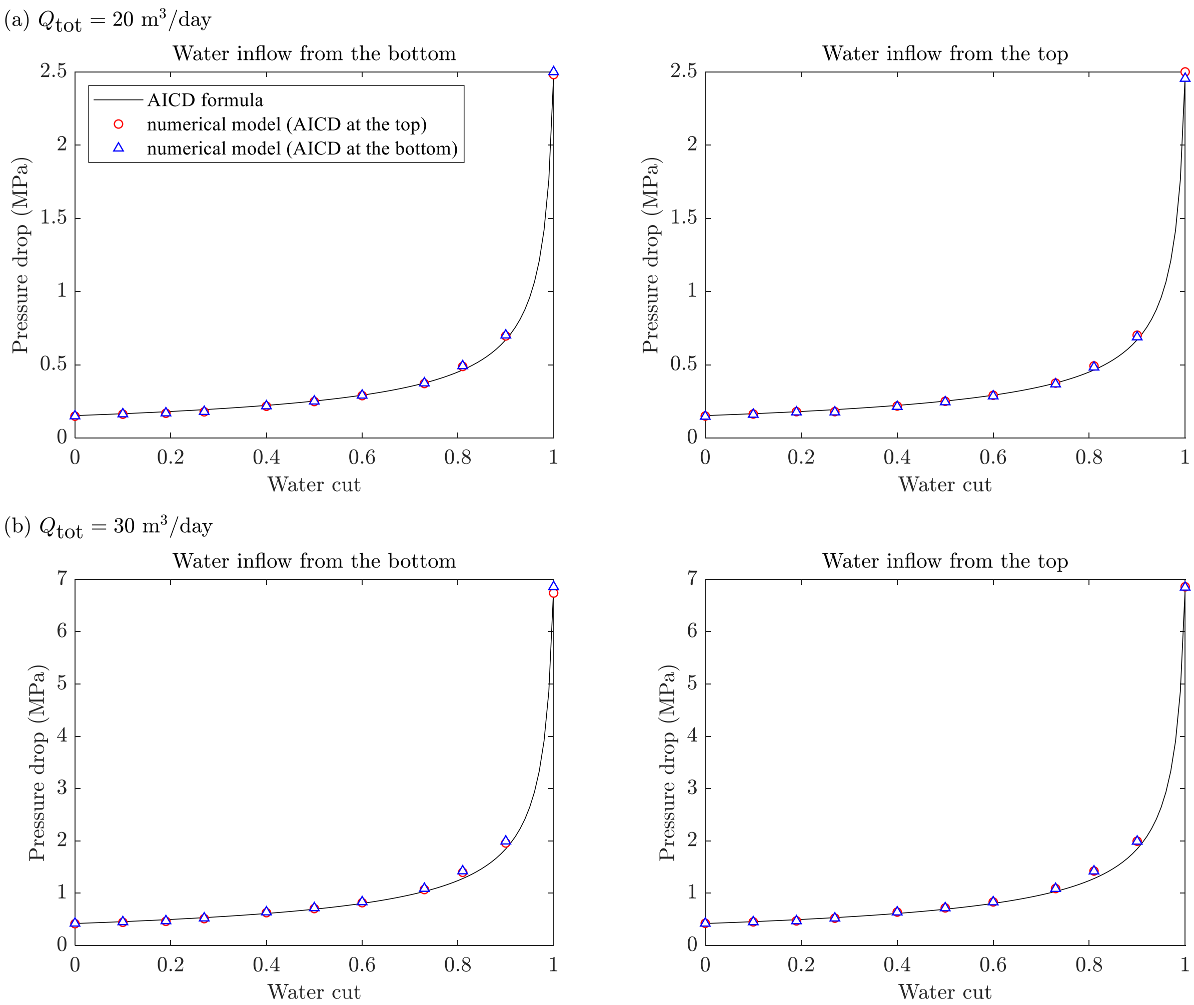

Fig. 11. Pressure drop imposed by the single AICD (either located at the top or the bottom of the annulus) for different water cut inflow scenarios with a total flow rate of Q_{tot} = (a) 20 or (b) 30 m^3/day. The left panel corresponds to the case that water inflows from the lower region of the annulus, while the right panel corresponds to the case that water inflows from the upper region of the annulus.

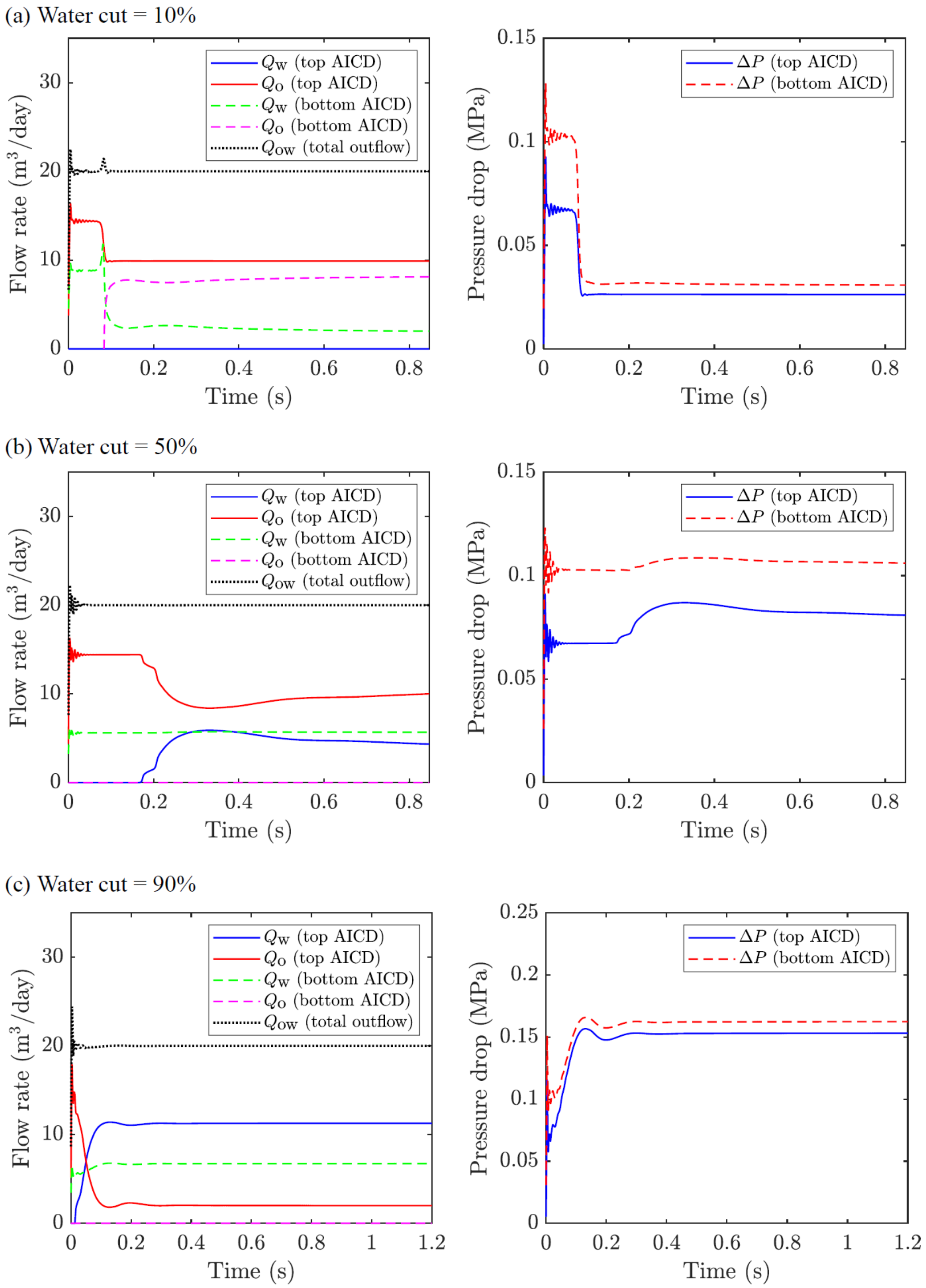

Fig. 12. Variation of flow rate (left) and pressure drop (right) at the two AICDs for different water cut cases with the total flow rate Q_{tot} = 20 m^3/day.

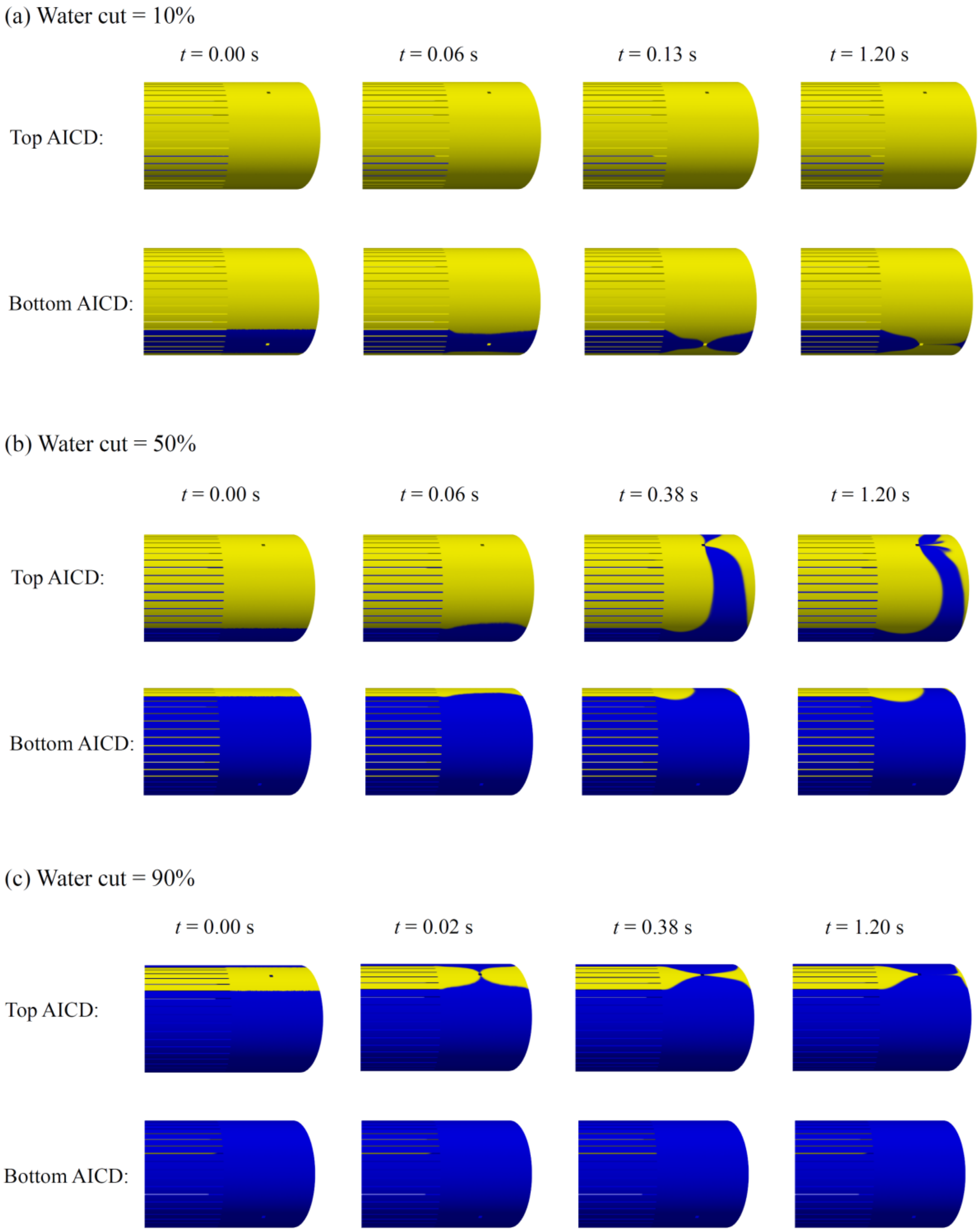

Fig. 13. Variation of flow pattern at the two AICDs for different water cut cases with the total flow rate Q_{tot} = 20 m^3/day.

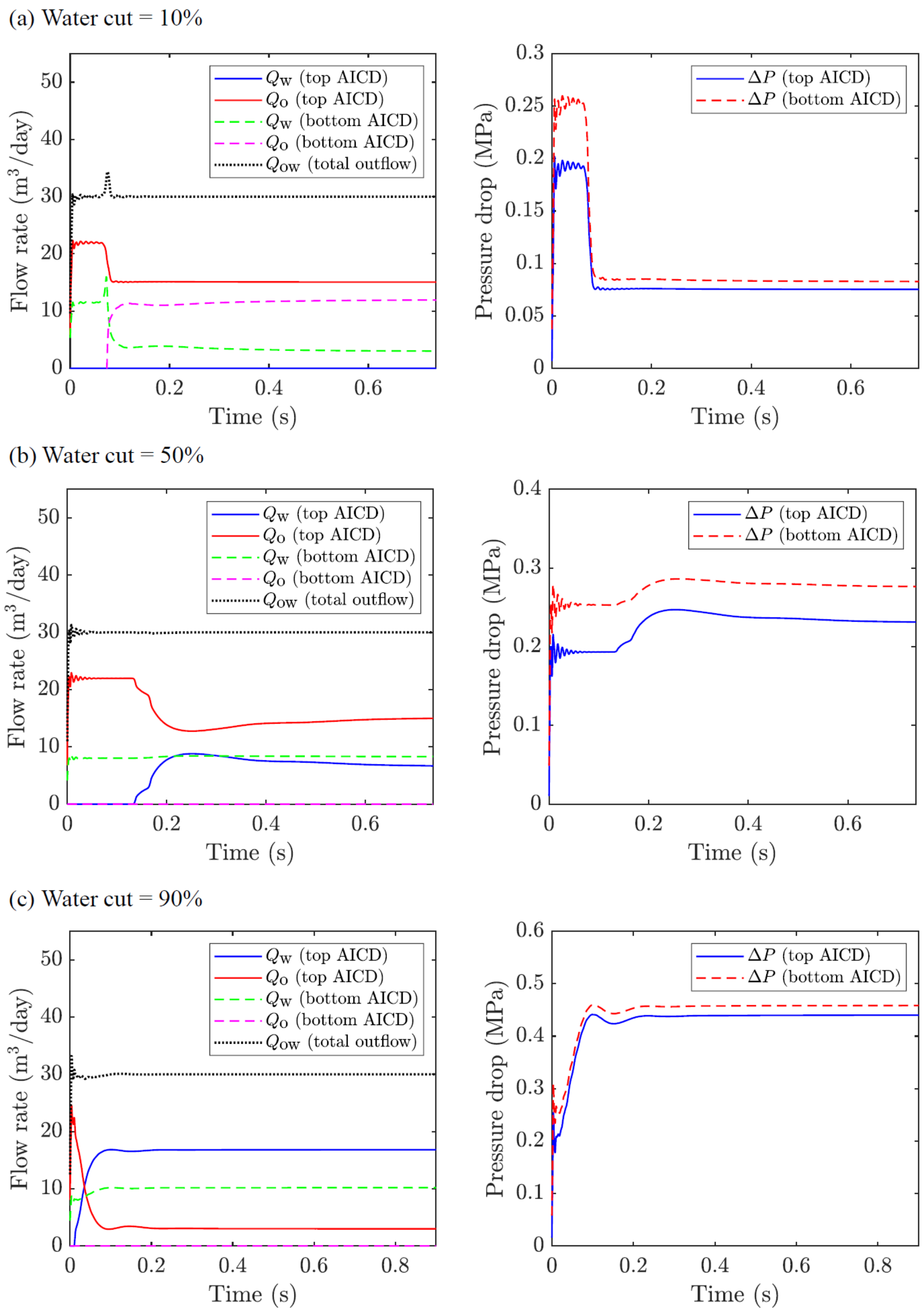

Fig. 14. Variation of flow rate (left) and pressure drop (right) at the two AICDs for different water cut cases with the total flow rate Q_{tot} = 30 m^3/day.

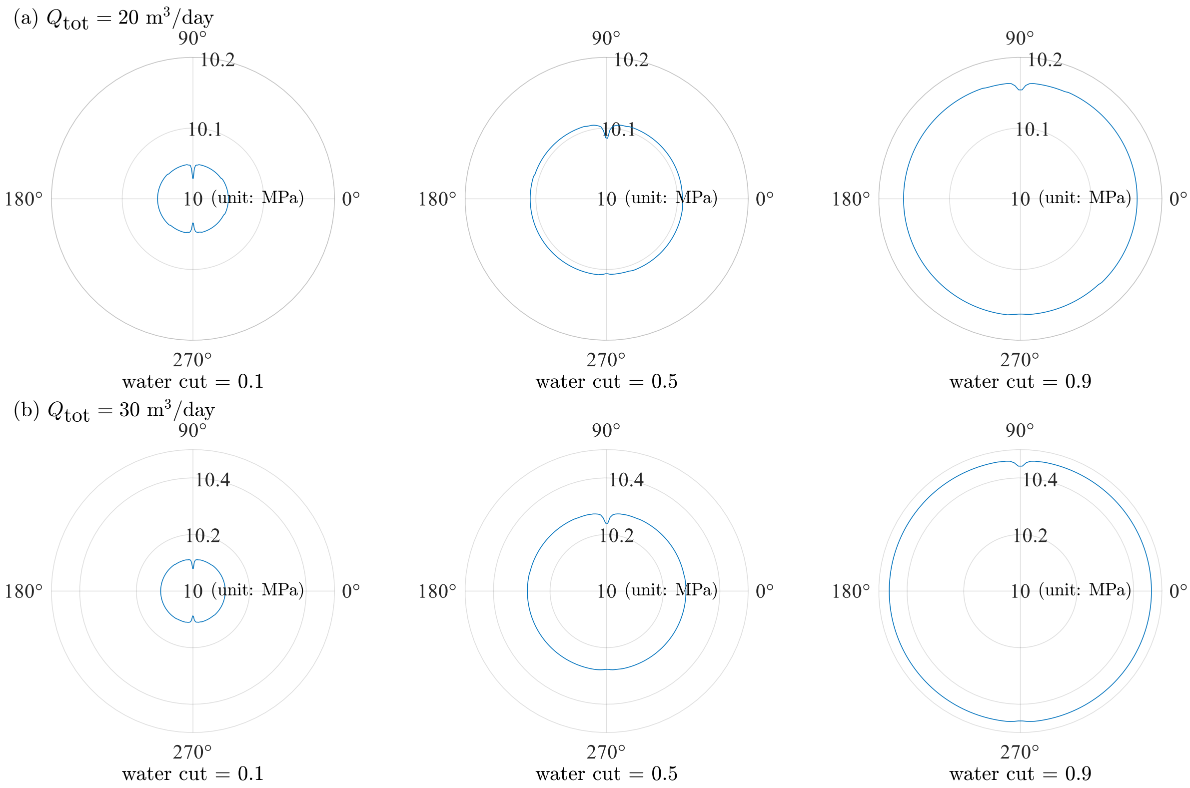

Fig. 15. Polar diagrams showing the variation of absolute pressure in the cross-section across the two AICDs. The values at 90° and 270° indicate the absolute pressure in the vicinity of the top and bottom AICDs, respectively. The absolute pressure in the tubing is 10 MPa.

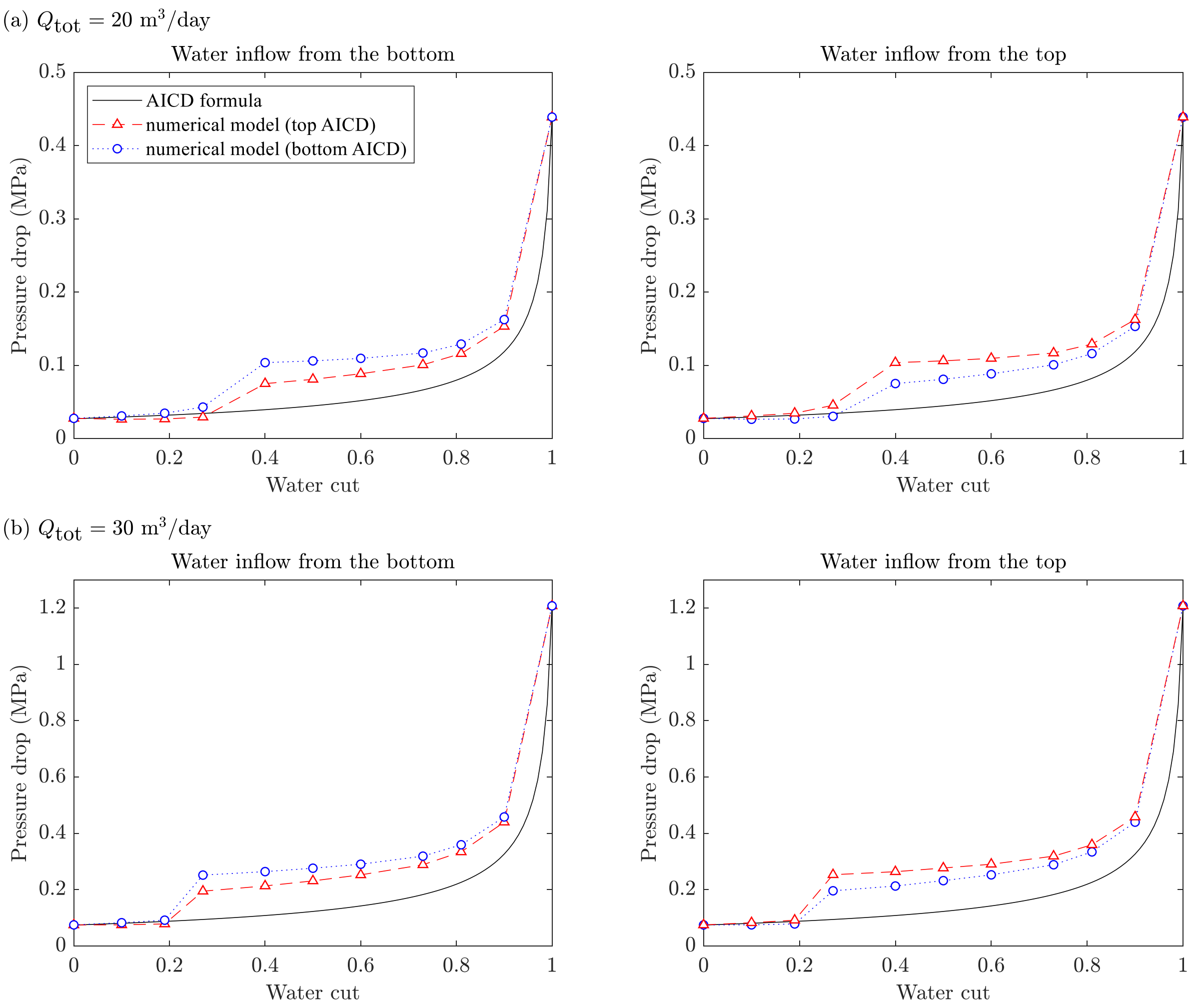

Fig. 16. Pressure drop imposed by the two AICDs (one is installed at the top and the other is installed at the bottom of the annulus) for different water cut inflow scenarios with a total flow rate of Q_{tot} = (a) 20 or (b) 30 m^3/day. The left panel corresponds to the case that water inflows from the lower region of the annulus, while the right panel corresponds to the case that water inflows from the upper region of the annulus.

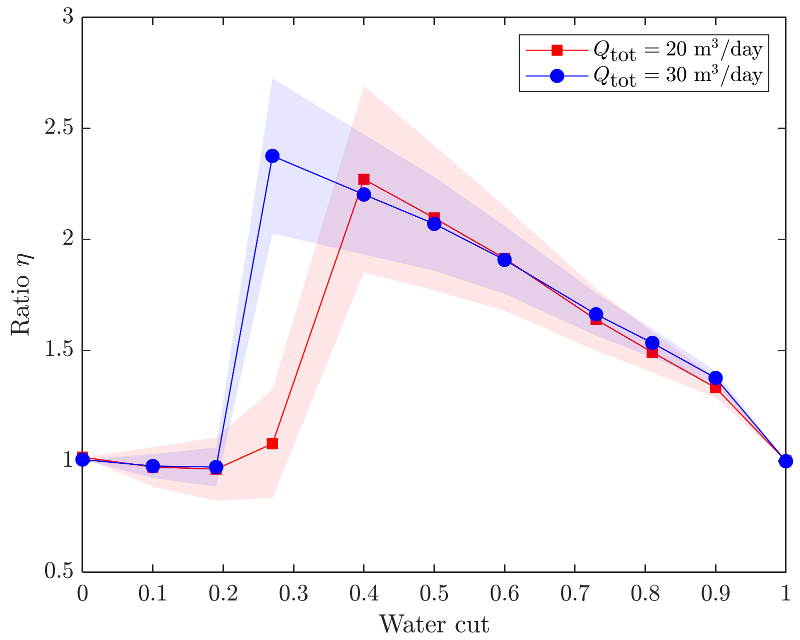

Fig. 17. Variation of the ratio η of the pressure drop derived from numerical simulation to that predicted from the AICD formula with respect to different water cut inflow conditions; the shaded areas indicate the variation induced by the location of the AICD and the condition that water enters the annulus from the top or bottom.

Table 1. Parameters of the completion joint.

Parameters	Value	Unit
Total length of the completion joint L	12.0	m
Diameter of the outer annulus D_o	0.24	m
Length of the inner annulus L_i	5.0	m
Mean diameter of the inner annulus D_i	0.14	m
Length of the narrow channel L_c	4.5	m
Cross-sectional area of the narrow channel A_c	4.8×10^{-5}	m^2
Hydraulic diameter of the narrow channel d_c	0.0046	m
Gap thickness of the inner annulus h_i	0.0027	m
Length of the closed region of the joint L_x	7.0	m
Reference fluid pressure inside the tubing p_0	1.0×10^{7}	Pa
Gravitational acceleration g	9.8	m/s^2

Table 2. Parameters of the fluids (based on the reference pressure $p_0 = 1.0\times10^7$ Pa).

Parameters	Value	Unit
Dynamic viscosity of oil μ_o	0.05	Pa·s
Density of oil ρ_{o0}	950.0	kg/m^3
Compressibility coefficient of oil c_o	7.25×10^{-10}	1/Pa
Dynamic viscosity of water μ_w	6.5×10^{-4}	Pa·s
Density of water ρ_{w0}	1040.0	kg/m^3
Compressibility coefficient of water c_w	3.55×10^{-10}	1/Pa
Interfacial tension σ	0.03	N/m
Total inflow rate at a single completion joint Q_{tot}	20.0 or 30.0	m^3/day
Water cut of the inflow Q_w/Q_{tot}	between 0.0 and 1.0	-

Table 3. Parameters of the AICD valve.

Parameters	Value	Unit
Strength parameter a_{AICD}	1.5×10^{-5}	-
Volume exponent m	2.5	-
Viscosity exponent n	0.6	-
Calibration density ρ_{cal}	1000	kg/m^3
Calibration dynamic viscosity μ_{cal}	5.0×10^{-4}	Pa·s
Cross-sectional area A_{AICD}	1.6×10^{-5}	m^2